Role of Fiber Thickness and Surface Treatment of Electrospun Polycaprolactone Matrices on the Growth of Different Breast Cancer-Associated Cells

Sankaranarayanan Sivakumar, Rafael Schmid, Annalena Wieland, Pamela L. Strissel, Reiner Strick, Lena Fischer, Ingo Thievessen, Elmar Kataev, Andreas Arkudas, Raymund E. Horch, Dirk W. Schubert, and Annika Kengelbach-Weigand*

Cancer models mimicking the tumor microenvironment are necessary to successfully develop and predict responses of oncological drugs. In this study, electrospun polycaprolactone (PCL) matrices are tested for the development of an in vitro breast cancer model. The effects of fiber thickness and plasma-treatment of the matrices on in vitro growth of breast cancer-associated cells, namely breast cancer cells MDA-MB-231, primary adipose-derived stem cells (ADSCs) and primary endothelial progenitor cells (EPCs) are evaluated. Surface treatment of the matrices by air-plasma leads to increased oxygen/carbon ratio and hydrophilicity. WST-8 analysis reveals that the proliferation of all three cell types increased exponentially over 12 d on all matrices. MDA-MB-231 and ADSC show a higher proliferation on nanofibers due to enhanced cellular adhesion compared to microfibers. In contrast, EPCs show a significantly higher proliferation on microfibers than on nanofibers at day 12 which can further be significantly improved by air-plasma treatment. Cross-sectioning analysis shows that cells grow on the surface of nanofibers, while microfibers have considerable cellular infiltration. These findings suggest that the electrospun PCL matrices are a suitable tool for the development of breast cancer models containing several cell types, which can ultimately lead to designing novel tumor therapies.

1. Introduction

Breast cancer remains the foremost female malignancy and reconstructive surgery in conjugation with radiotherapy is the current gold standard therapy.[1] Experimental models to study this tumor attempt to reconstitute the tumor microenvironment in vitro and in vivo, in order to develop platforms for studying tumor genetics, cell biology[2] and drug screening toward designing novel therapies.[3] Numerous 3D in vitro breast cancer models have been established and validated using a combination of hydrogels and scaffolds, through technologies such as microfluidics,[4] 3D printing[5] and spheroid cultures.[6] In vivo breast cancer models could be patient-derived xenografts (PDXs),[7] cell-line derived xenografts (CDXs)[8] or genetically engineered mouse models.[9] While PDXs are obtained by implanting patient-derived tumor tissues and are potentially heterogeneous, CDXs are obtained by implanting human and animal-derived breast cancer cell lines in an artificial matrix but are predominantly homogeneous. Although CDXs have inferior clinical therapeutic predictability in comparison to PDXs, they are helpful in studying tumor biology and screening anti-tumorigenic and anti-angiogenic drugs for their efficacy against well-characterized breast cancer cell lines. [8,10]

Polycaprolactone (PCL) is a biodegradable, hydrophobic polymer widely used in tissue engineering research for applications such as cornea,[11] nerve,[12] skin,[13] bone, cartilage, muscle

S. Sivakumar, R. Schmid, A. Arkudas, R. E. Horch,
A. Kengelbach-Weigand
Department of Plastic and Hand Surgery
Laboratory for Tissue Engineering and Regenerative Medicine
University Hospital Erlangen
Krankenhausstraße 12, 91054 Erlangen, Germany
E-mail: annika.kengelbach-weigand@uk-erlangen.de

A. Wieland, P. L. Strissel, R. Strick
Department of Gynecology and Obstetrics
University Hospital Erlangen
Universitätsstraße 21-23, 91054 Erlangen, Germany

L. Fischer, I. Thievessen
Department of Biophysics
Friedrich-Alexander University of Erlangen-Nürnberg (FAU)
Henkestraße 91, 91052 Erlangen, Germany

E. Kataev
Department of Chemistry and Pharmacy
Friedrich-Alexander University of Erlangen-Nürnberg (FAU)
Nikolaus-Fiebiger-Str. 10, 91058 Erlangen, Germany

D. W. Schubert
Institute of Polymer Materials
Friedrich-Alexander University of Erlangen-Nürnberg (FAU)
Martensstraße 7, 91058 Erlangen, Germany

Table 1. Optimized parameters for electrospinning of PCL.

Matrices	Solvent system	Polymer (PCL) concentration [% w/v]	Flow rate [mL h^{-1}]	Needle-to-collector distance [cm]	Voltage over the needle and the collector [kV]	Fiber diameter (mean ± SD) [nm]
Random-nanofibers	Formic acid:acetic acid (7:3)	12% (80 kDa)	0.2	17	15	125 ± 32
Random-micro/nano fibers	Chloroform:ethanol (7:3)	10% (80 kDa) and 4% (14 kDa)	2	24	20	1570 ± 383 / 462 ± 173
Random-microfibers	Chloroform	17.5% (80 kDa)	3.6	15	15	8801 ± 716
Aligned-nanofibers	Chloroform:ethanol (7:3)	10% (80 kDa) and 4% (14 kDa)	2	24	20	865 ± 104

and cardiovascular tissue engineering.[14] In addition, PCL and other polymeric scaffolds are also used in breast tumor engineering applications, which share properties with tissue engineering such as development of cell-matrix interactions and tissue growth.[15] More specifically, researchers have attempted to establish 3D engineered PCL as a component of extracellular matrix (ECM) for the development of in vitro and in vivo breast cancer models.[16]

A number of breast cancer cell lines have been generated as experimental models to study subgroups of breast cancer and its biology. [17] Triple-negative breast cancer (TNBC) are highly malignant and have the poorest prognosis. Out of the 27 most widely studied TNBC cell lines, MDA-MB-231 is the most widely studied.[18] Increased expression of tumor-associated genes in breast cancer cell lines have been reported in co-culture with adipose-derived stem cells (ADSC),[19] whose interactions with breast cancer cells and tumor progression has been studied extensively.[20] Endothelial progenitor cells (EPC) are a collection of many subtypes of cells that play a crucial role in tumor angiogenesis.[21] Successful cytocompatibility testing of electrospun PCL fibers have been previously reported with MDA-MB-231[22] or MCF-7,[23] ADSC,[24] and EPC.[25] Hence, it is of interest to further characterize the interaction of breast cancer cell lines, ADSC and EPC with PCL toward development of an in vitro breast cancer model.

The aim of this study is to characterize the effect of fiber diameter and surface treatment of the electrospun PCL matrices toward application as in vitro breast cancer model. Although based on the application of different cell types, several studies have declared contrasting results, where either nanofibers[26] or microfibers[27] have been shown to support better cell growth, or no significant effect of the fiber diameter was found.[28] This leads to a conclusion that the influence of the fiber diameter could be tissue- and cell-specific. For improving the hydrophilicity, surface treatment such as plasma treatment,[29] ultraviolet (UV) irradiation[30] ion sputtering and corona discharge of PCL scaffolds were recently introduced. These techniques enhance properties such as wettability, which influence matrix adhesion and cellular biocompatibility. Plasma treatment has been shown to improve cell growth in applications like bone,[29a,b,31] cartilage,[32] skin[29d] and vascular tissue regeneration.[33]

In this study, we tested the growth of breast cancer cells MDA-MB-231 and the breast-associated cell types ADSC and EPC, on PCL nanofiber and microfiber matrices, with and without plasma treatment. Our future goal is to develop optimized matrices for in vitro and in vivo CDX/PDX breast cancer models.

2. Results
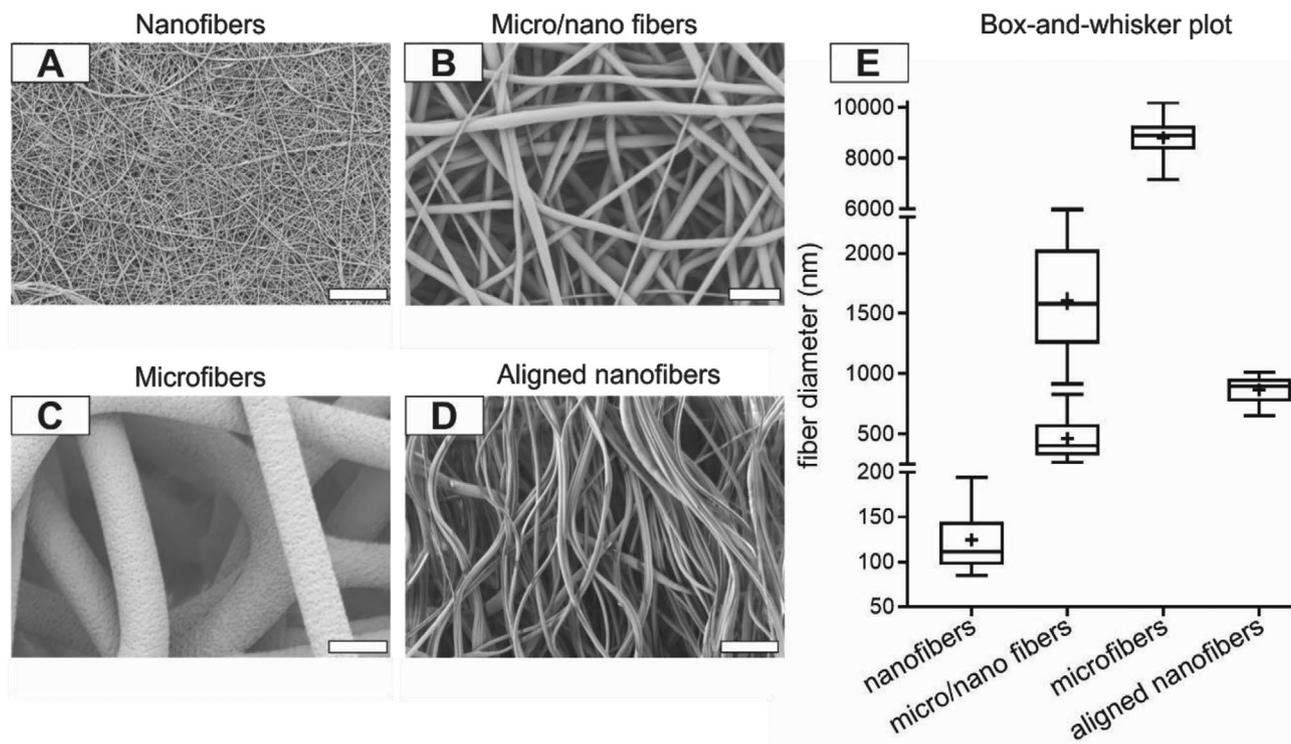
2.1. Analysis of Electrospun PCL Matrices

Random and aligned fibers of different diameters were produced by varying the electrospinning parameters (**Table 1**). **Figure 1** shows representative scanning electron microscopy (SEM) images and fiber diameter distribution of the different matrices. The mean PCL fiber diameters were the following: nanofibers: 125 ± 32 nm (Figure 1A), micro/nanofibers: 1570 ± 383 nm / 462 ± 173 nm (Figure 1B), microfibers: 8801 ± 716 nm (Figure 1C), aligned nanofibers: 865 ± 104 nm (Figure 1D). The micro/nanofiber matrices were bimodal with microfiber and nanofiber components. Figure 1E shows the mean, median and range of the fiber diameters of each type. The electrospun nanofiber and microfiber matrices were spun to a thickness of 17 ± 3 µm and 283 ± 15 µm respectively, which could be handled with 24-well cell crowns. The formic acid/acetic acid solvents degraded the PCL within a day, and hence fresh polymeric solutions were prepared and electrospun within a day for the nanofibers, while PCL solution prepared in chloroform and ethanol as solvents were stable for at least two weeks.

Tensile properties of the electrospun matrices are reported in Table S1 (Supporting Information). Microfibers had lower "Young's modulus" of 8.51 ± 1.46 MPa and higher "strain-at-break" of 460.74 ± 111.71%, while the corresponding values of nanofibers are 32.91 ± 4.21 MPa and 128.99 ± 10.9%. Aligned-nanofibers had a "Young's modulus" of 17.79 ± 7.32 MPa along the fiber direction.

2.2. Surface Treatment of Electrospun PCL Matrices

The surface treatment of electrospun PCL matrices by air-plasma and UV treatments and their effects on surface properties of the matrices such as hydrophilicity, morphology and adhesion of fluorescent collagen-fibrinogen and rat-tail collagen-I were studied.

The pristine electrospun nanofibers and micro/nanofibers had a mean water-contact angle (WCA) of 114.5° and 126.8° respectively. All plasma-treated samples showed a transition from an initial hydrophobic behavior toward increasing hydrophilicity, but WCA could not be measured as the water droplets were absorbed by the matrices. The effects on morphology of the fibers and fluorescent staining of the surface coatings due to air-plasma treatment are summarized in **Figure 2**. On both the nanofiber and micro/nanofiber

**ADVANCED
SCIENCE NEWS**
www.advancedsciencenews.com

**ADVANCED
MATERIALS
INTERFACES**
www.advmatinterfaces.de

Figure 1. SEM images of electrospun PCL fibers. A) Nanofibers, B) micro/nanofibers, C) microfibers, D) aligned nanofibers, E) box-and-whisker plot showing diameters of the fibers [mean (+), median, interquartile range and range (max, min)]. The nanofibers and microfibers components of the bimodal micro/nanofibers are plotted separately (scale bar = 10 µm).

matrices, after 150 s of treatment, the fibers still retained their morphology (Figure 2A,D). After 300 s of treatment, pockets of fiber-melting could be observed in nanofiber matrices (Figure 2B,E). After 450 s of treatment, significant melting of the matrices could be observed (Figure 2C,F). Hence, for the subsequent cell culture studies, 150 s of air plasma treatment was chosen as the optimal plasma-exposure time. Independent of plasma treatment, adhesion of rat-tail collagen-I could be observed on both pristine and plasma-treated nanofiber and micro/nanofiber matrices by anti-collagen-I immunofluorescence staining (Figure 2G–J).

X-ray photoelectron spectroscopy (XPS) analysis of the micro/nanofiber matrices after 150 s of air-plasma treatment is presented in **Figure 3**. C1s spectrum of pristine sample was described by spectral components related to different carbon atoms in PCL, C−C at 285.0 eV, C−O at 286.6 eV and O=C−O at 289.0 eV. Calculated atomic concentrations approximately correspond to PCL stoichiometry. Air-plasma treatment resulted in a reduction in atomic concentration of carbon, and an increase in concentration of oxygen and nitrogen, due to introduction of C=O and C−N groups indicated at 287.8 and 285.8 eV binding energy respectively.

The samples were exposed to UV for 60, 180, and 300 s. The mean WCA measurements for these different UV exposure times on nanofibers were 112.7°, 58.6°, and ≈0°, respectively, indicating increasing hydrophilicity with increasing treatment times. However, on both nanofiber and micro/nanofiber matrices significant melting or disintegration could be observed after 60 s or longer times of treatment (Figure S1,

Supporting Information). Although, UV treatment also resulted in increased hydrophilicity and collagen-fibrinogen adhesion, plasma treatment of the matrices was considered for further experiments, as samples treated with UV melted or disintegrated at much shorter time (60 s) as compared to plasma-treated samples (longer than 300 s) before considerable hydrophilicity could be achieved.
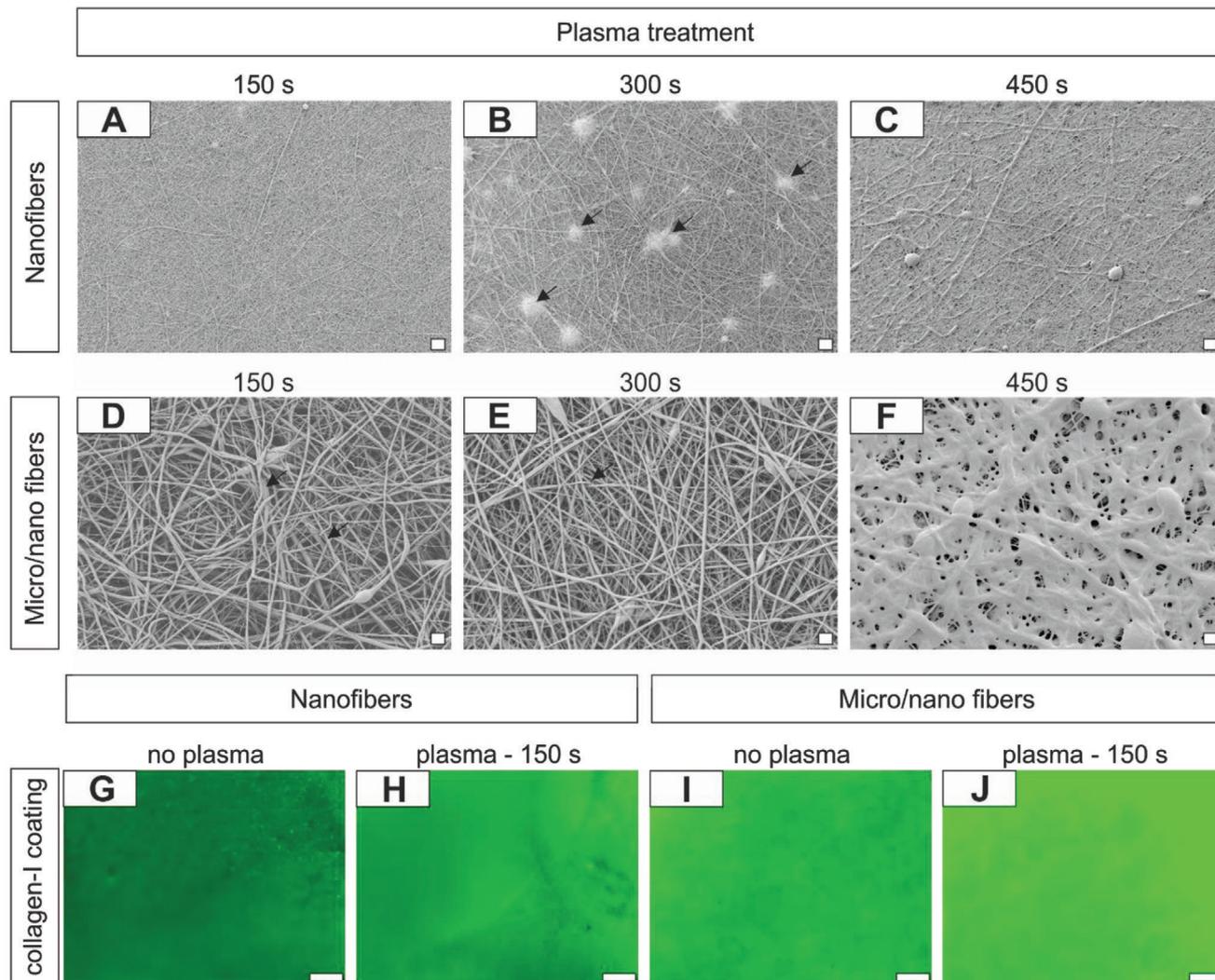
2.3. Effects of Fiber Diameters and Air-Plasma Treatment on the Behavior of Breast Cancer-Associated Cells

The effects of fiber diameters (nanofibers vs microfibers), orientation (random vs aligned) and air-plasma treatment (hydrophobic vs hydrophilic) on the growth of the breast cancer-cell line MDA-MB-231, and two breast cancer-associated cell types ADSC and EPC were studied.

All three cell types were completely retained and adherent upon seeding on the random- and aligned-nanofibers. However, microfibers had lower cell adhesion, which was observed by leakage of cells through the inter-fiber pores during the seeding process.

2.3.1. MDA-MB-231

MDA-MB-231 adhered and proliferated on all random and aligned PCL matrices. The rate of proliferation of was lower on the 3D matrices than on 2D tissue culture plates (Figure S2,

**ADVANCED
SCIENCE NEWS**
www.advancedsciencenews.com

**ADVANCED
MATERIALS
INTERFACES**
www.advmatinterfaces.de

Figure 2. Air-plasma-treatment of electrospun PCL fibers. SEM images of the nanofibrous and micro/nanofibrous matrices after A,D) 150 s, B,E) 300 s, C,F) 450 s of plasma treatment (scale bar = 10 µm, black arrows indicating regions of fiber-melting). Immunofluorescence imaging of the rat-tail collagen-I coated matrices G,I) before and H, J) after plasma treatment for 150 s by anti-collagen-I staining (scale bar = 100 µm).

Supporting Information). **Figure 4** describes the proliferation of MDA-MB-231 cells on the different matrices measured on days 3, 6, 9, and 12; the 4′,6-diamidino-2-phenylindole (DAPI)/actin fluorescent staining and cross-section analysis on Day 12. The exponential increase in cellular proliferation, measured by the WST-8 assay, was similar on all matrices irrespective of fiber thickness (nanofibers, micro/nanofibers or microfibers), orientation (random or aligned), or the degree of hydrophilicity (hydrophilic or hydrophobic) (Figure 4A). A significantly higher proliferation on plasma-treated nanofibers than on plasma-treated microfibers ($p < 0.05$) was observed. Top view of the surface of nanofibers, micro/nanofiber, and aligned-nanofiber matrices, observed by DAPI/actin staining and scanning electron microscopy (SEM) in Figure 4B–D, shows cells growing on the surface of these matrices, with alignment of cellular actin along the nanofiber direction on aligned nanofibers. Cross-section analysis (Figure 4E–G) of the matrices, with a merge of phase-contrast and actin/DAPI staining images, showed that

layers of cells grew only on the surface of nanofiber and micro/nanofiber matrices without migrating (≤20 µm) into them. In contrast, microfiber matrices showed considerable cell migration throughout the matrices (≥ 200 µm) by day 12. The cellular infiltration in microfibers is also shown by confocal microscopy till a depth of 41.59 µm on the microfiber matrices (Figure S3, Supporting Information).

Further characterization of the growth of MDA-MB-231 on the matrices is displayed in **Figure 5**. Fluorescence ubiquitination cell cycle indicator (FUCCI)-transfected MDA-MB-231 indicated that the cells on the matrices were proliferating and undergoing the different phases of cell cycle (Figure 5A), where cells in green indicate S, G2 and M phases, cells in red indicating G1 phase and cells in yellow representing G1/S transition. The ratio of green:red:yellow cells were found to be 0.81:0.19:0 on nanofibers and 0.57:0.4:0.03 on microfibers. Cell growth could be observed on the surface of the nanofiber matrices (Figure 5B) and within the microfibrous matrices
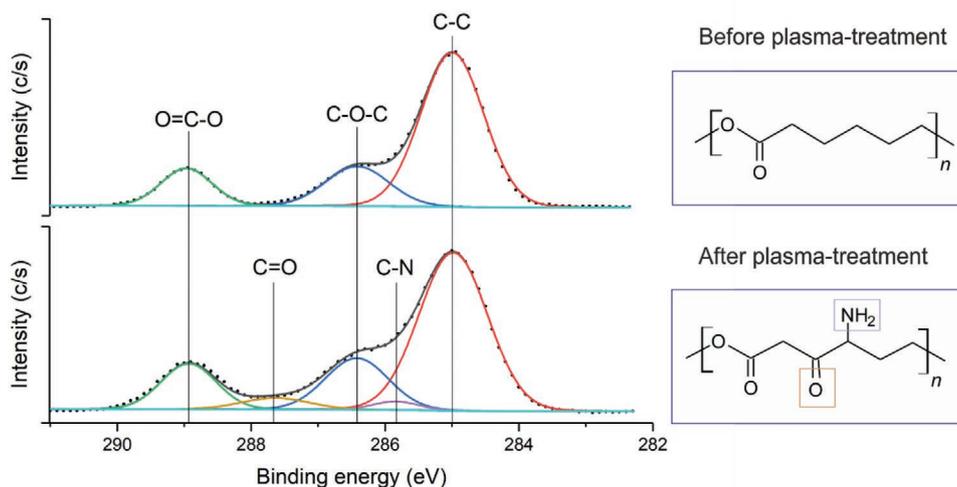
Figure 3. C1s spectrum of XPS analysis, corresponding chemical structures, and atomic concentrations of PCL micro/nanofibers before and after plasma treatment.

(Figure 5C) by day 6. After day 12, MDA-MB-231 that were cultured on 2D-tissue culture plates and on the different PCL matrices were extracted and cultured on low-adhesion plates, to form mammospheres. The mammosphere forming index (MFI, Figure 5D), which identifies and indicates the proliferation of cancer stem cells (CSC) within the MDA-MB-231 cells, was calculated from the cells extracted from the different matrices (Figure 5E–H). The MFI of the cells extracted from PCL matrices was found to be similar to that of cells from 2D-tissue culture plates. The SEM images of all three cell types grown on the nanofibers and microfibers matrices were included in Figure S4 (Supporting Information).

2.3.2. Adipose-Derived Stem Cells and Endothelial Progenitor Cells

ADSC and EPC were cultured on random-oriented PCL nanofibers and microfibers and aligned-nanofibers. Both cell types adhered and proliferated on the matrices over time (**Figures 6** and **7**).

The exponential growth of ADSC was similar on both random- and aligned-nanofibers over 12 d (Figure 6A). Significantly higher proliferation on plasma-treated nanofibers than on plasma-treated microfibers ($p < 0.05$) was observed over 12 d. Nevertheless, exponential growth of cells was also observed on microfibers. Similar growth of ADSC on hydrophobic or plasma-treated hydrophilic surfaces were observed. Cell growth on the surface of random- and aligned-nanofibers could be observed by the fluorescent staining of actin/DAPI (Figure 6B,C), where the alignment of cellular actin could be observed to be along the nanofiber direction in the latter. Cross-sectional analysis (Figure 6D,E) of the matrices revealed that ADSC formed a monolayer on the surface of nanofiber matrices and infiltrated throughout the microfiber matrices (≥ 200 µm).

Similar to ADSC, EPC also showed a similar exponential growth on both nanofiber and microfiber matrices over day 12 (Figure 7A). However, the proliferation of EPC was significantly higher on microfibers than on nanofibers. Further significant enhancement of EPC proliferation was observed on plasma-treated hydrophilic microfibers than on pristine microfibers. Cell growth could be observed on the surface of random- and aligned-nanofibers (Figure 7B,C) with actin alignment along the nanofiber direction in the latter. Cross-sectional analysis (Figure 7D,E) of the matrices revealed that EPC formed a monolayer on the surface of nanofiber matrices, but infiltrated throughout the microfiber matrices (≥ 200 µm).

3. Discussion

In vitro and in vivo breast cancer models are critical in the development and validation of novel therapies against breast cancer.[9,34] Bioengineering strategies have led to the development of fibrous scaffolds that mimic tumor microenvironment and heterogeneity with high fidelity.[6a] Biocompatibility of PCL for the growth of MDA-MB-231 cells[22b,c,23,35] and other breast cancer-associated cell types used in this study such as ADSC[24,36] and EPC[25,37] have previously been reported. Breast cancer cells cultured on electrospun PCL matrices enhanced their CSC properties, mammosphere-forming capability[22a] and epithelial to mesenchymal transitions,[16a,23,38] while cancer-associated fibroblasts induce increased invasiveness to tumors.[39] Culturing breast cancer cells on 3D matrices also enable better mimicking of the tumor microenvironment that the drug responses are more physiological, compared to cells grown on 2D surfaces.[5a,34a,c] These studies validate the use of electrospun PCL matrices for the development of in vitro and in vivo breast cancer models. The aim of this study was to characterize the effect of fiber-thickness and plasma treatment for enhancing the properties of the electrospun PCL matrices for the growth of various breast cancer-associated cell types, toward development of in vitro and in vivo CDX models.

In order to study the role of fiber-thickness, established electrospinning protocols from Stafiej et al.[11] and Balguid et al.[40] were used to generate PCL matrices with fibers of different
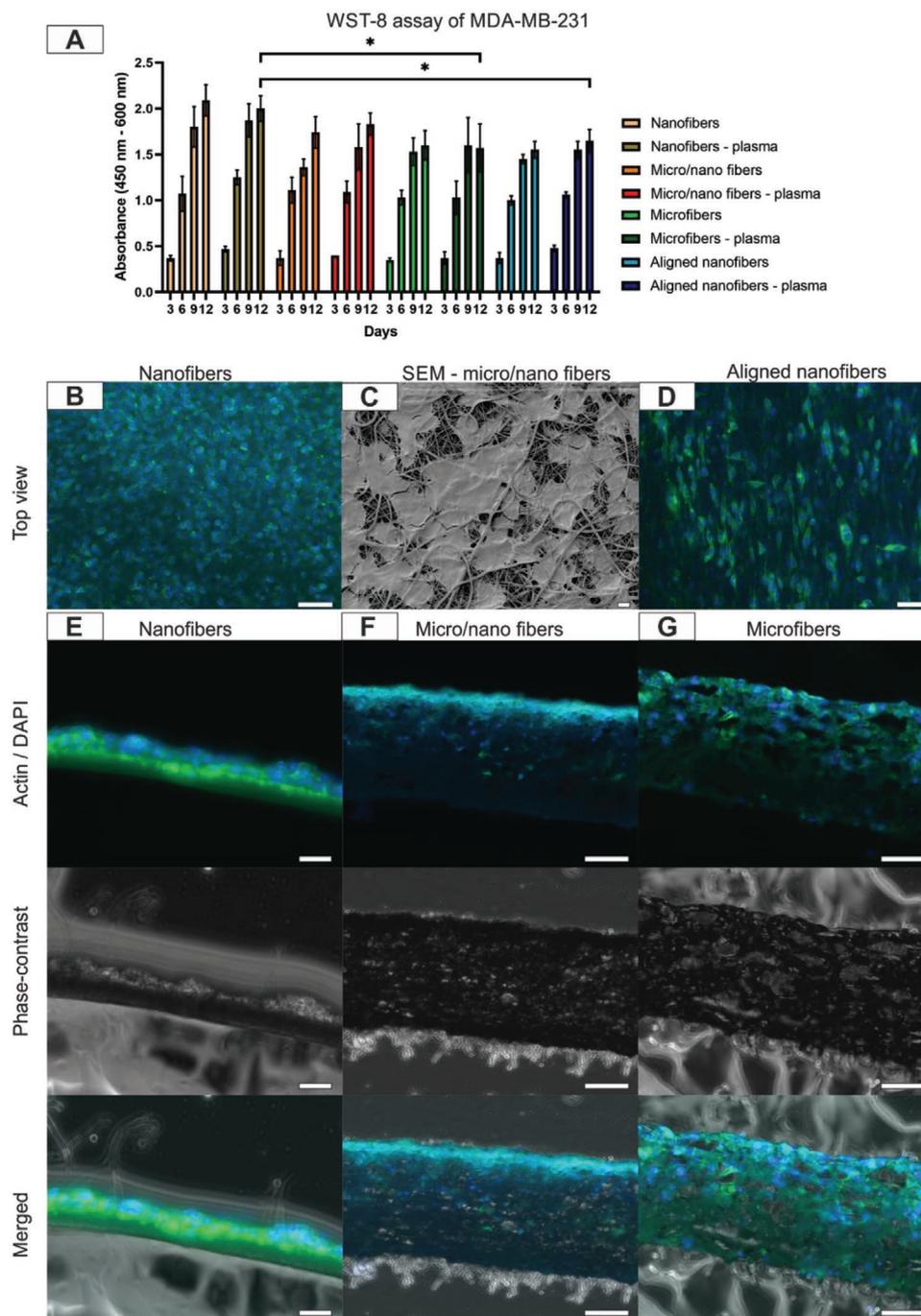
Figure 4. Proliferation of MDA-MB-231 cells on electrospun PCL matrices. A) Proliferation of MDA-MB-231 cells over 12 d measured by WST-8 assay on random-oriented and aligned PCL fibers with and without plasma treatment ($n = 3$, mean $\pm$ SD). Top view of B) cell growth on nanofibers, DAPI (blue) and actin (green) (scale bar = 100 µm); C) SEM images (day 8) on micro/nanofibers (scale bar = 10 µm); D) cell growth on aligned fibers, DAPI (blue) and actin (green) (scale bar = 100 µm). Cross-sectional analysis of the cellular migration of MDA-MB-231 (overlay of phase-contrast and DAPI (blue)/actin (green) staining) on E) nanofibers (scale bar = 50 µm), F) micro/nanofibers (scale bar = 50 µm), and G) microfibers (scale bar = 100 µm) (*$p < 0.05$).

diameters ranging from nanofibers (125 $\pm$ 32 nm) to microfibers (8801 $\pm$ 716 nm) respectively. In addition to unimodal nanofiber and microfiber matrices, bimodal micro/nanofibers were also generated through a combination of PCL of different molecular weights (80 and 14 kDa). Multi-modal fibers are formed due to jet splitting during electrospinning, and is

described as a function of viscosity and concentration of the polymer solution for a given flow rate in Schubert et al.[41] Bimodal fibers provide an intermediate surface area, compared to high surface area in nanofiber matrices and low surface area in microfiber matrices, per unit volume of the PCL matrix. The tensile properties of the electrospun matrices indicated that
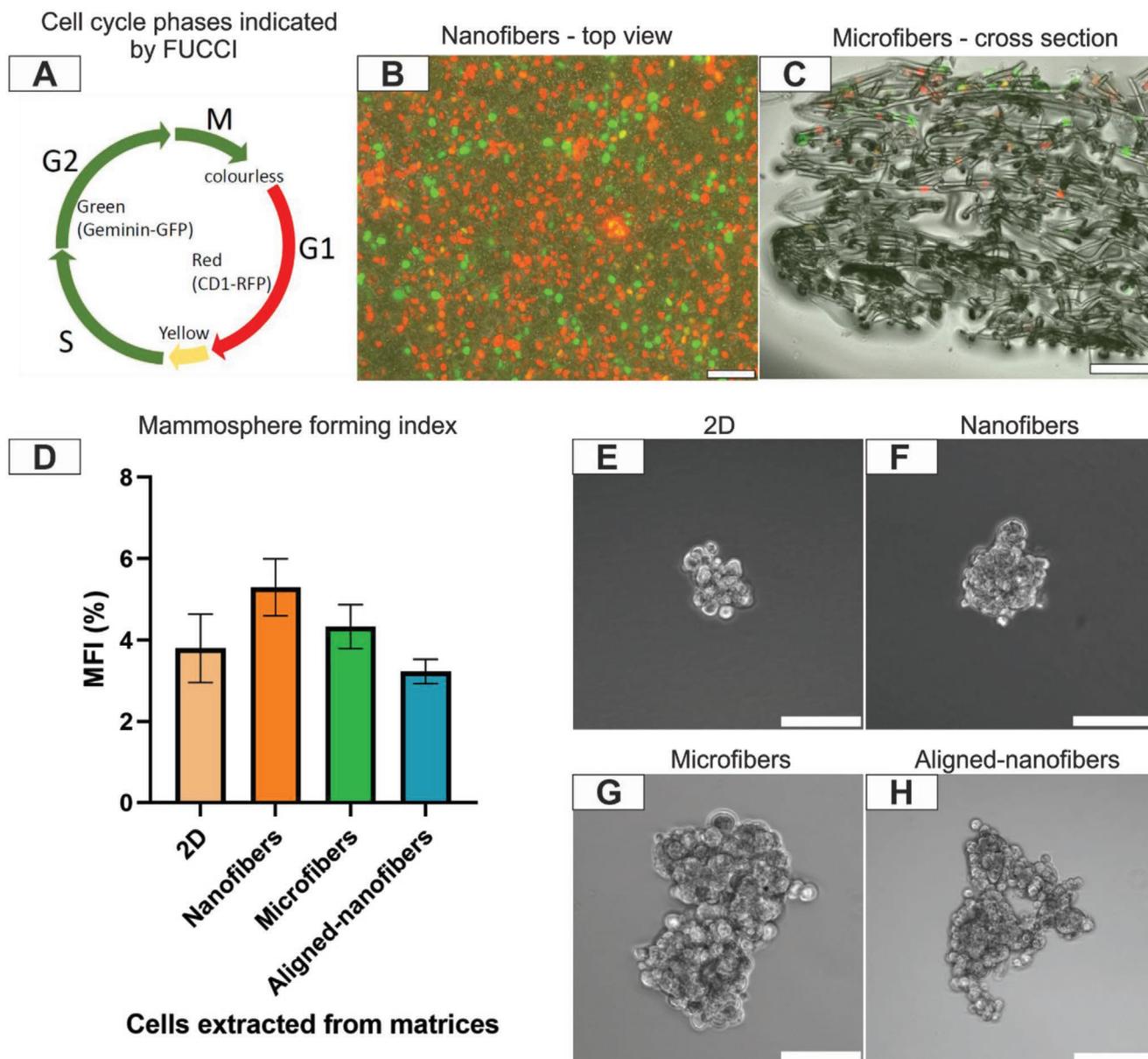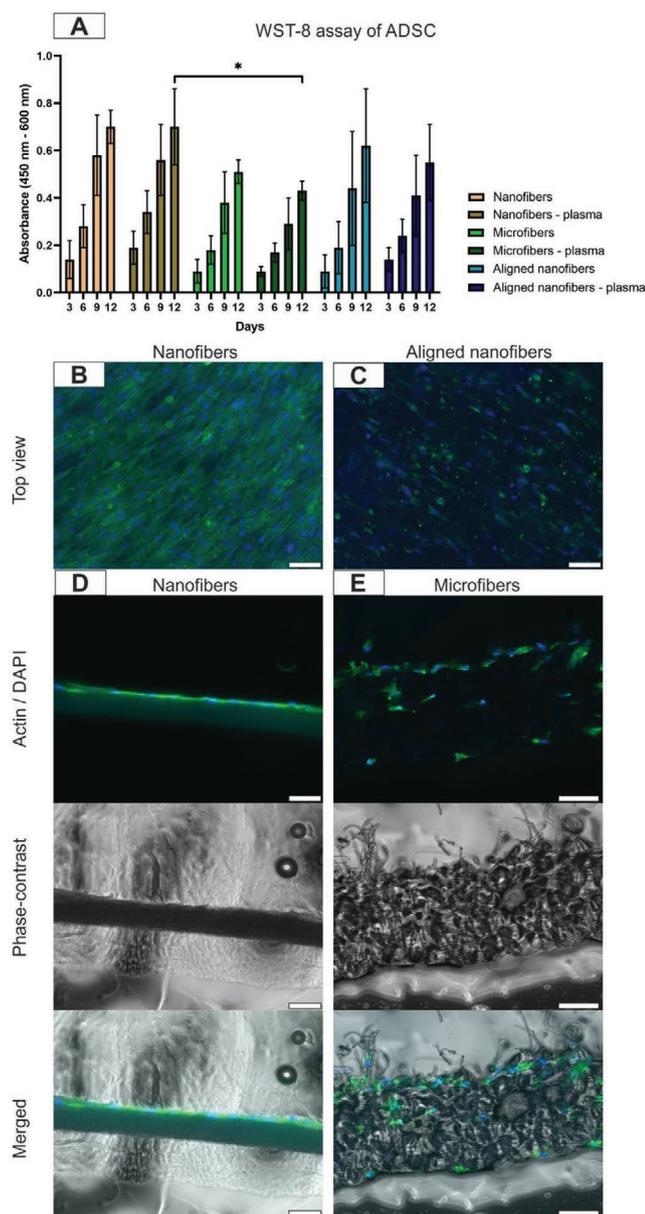
Figure 5. MDA-MB-231 cell growth on PCL matrices. Cultivation of FUCCI-transfected MDA-MB-231 cells on PCL matrices on day 6: A) cell cycle phases indicated by the FUCCI construct, B) top view of cell growth on the surface of nanofibrous scaffold (scale bar = 100 μm), C) cross-sectional analysis of cellular migration in microfibers (overlay of phase-contrast image and FUCCI-transfected cells) (scale bar = 100 μm). Mammosphere formation assay: D) Mammosphere forming index (n = 3, mean ± SD) of the cells extracted from E) 2D tissue culture plates, and PCL matrices F) nanofibers, G) microfibers, H) aligned nanofibers (scale bar = 100 μm).

microfibers had lower Young's modulus and higher strain-at-break, compared to nanofibers.

Guex et al.[42] recommends a matrix thickness of 200–300 μm for ease of handling during cell culture and histology, while the electrospun nanofiber and microfiber matrices in this study were spun to a thickness of about 17 ± 3 μm and 283 ± 15 μm respectively and could be handled with the 24-well cell crowns for cell culture. For cell culture on electrospun PCL matrices, all the pristine and plasma-treated matrices in this study were coated with 1 mg mL^{-1} of rat-tail collagen-I prior to cell seeding. Type-I collagen has been shown to be one of the most important components for the normal breast tissue development[43]

and an increased concentration of collagen-I within the breast tissue has been correlated to a higher risk of developing breast cancer.[22c,44] It further reinforces the mechanical and biological properties of electrospun PCL matrices and enhances efficiency of cell growth on PCL matrices.[45]

Certain studies have found that microfibers support the cell growth better than nanofibers,[27–28] while in other studies nanofibers were found to be more suitable.[26,46] These contrasting observations were explained based on matrix properties such as inter-fiber spacing,[27] focal adhesion complexes,[28,37d] surface area to volume ratio[26] and fiber flexibility.[26] This leads to a conclusion that the effect could be tissue-specific and factors

**ADVANCED
SCIENCE NEWS**
www.advancedsciencenews.com

**ADVANCED
MATERIALS
INTERFACES**
www.advmatinterfaces.de

Figure 6. Proliferation of ADSC on electrospun PCL matrices. A) Proliferation of ADSC over 12 d measured by WST-8 assay on random-oriented and aligned PCL fibers with and without plasma treatment ($n = 3$, mean ± SD). Top view of cell growth (DAPI (blue) and actin (green)) on B) nanofibers and C) aligned fibers (scale bar = 100 μm). Cross-sectional analysis of the cellular migration of ADSC (overlay of phase-contrast and DAPI (blue)/actin (green) staining) on D) nanofibers (scale bar = 50 μm) and E) microfibers (scale bar = 100 μm) (*$p < 0.05$).
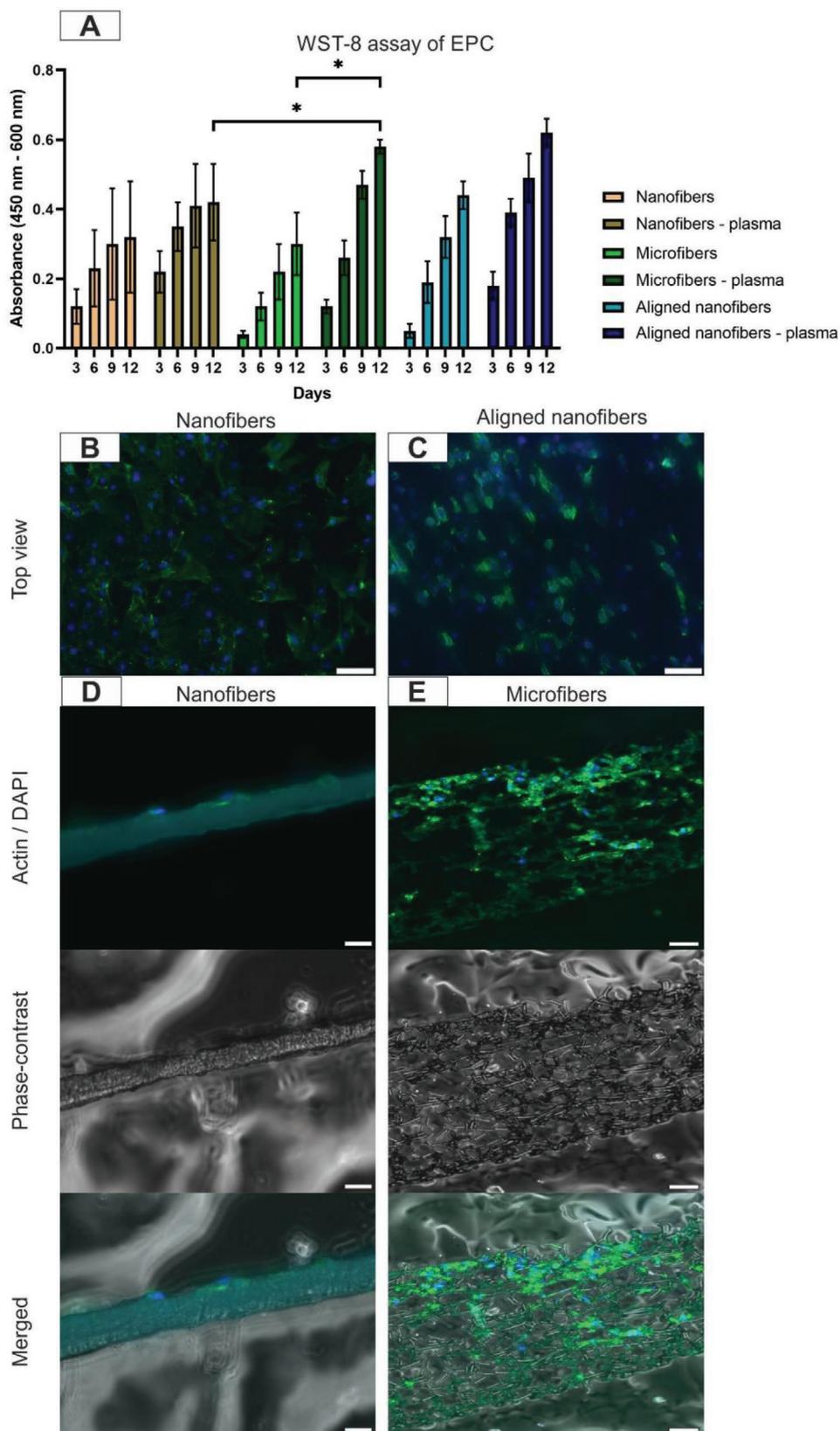
beyond fiber diameters such as cell seeding density, scaffold material, fiber alignment and media composition determine the cellular proliferation and behavior.[47] Since the fiber diameter affects various parameters such as cell proliferation, migration, cellular metabolism, viability and differentiation,[47–48] the effect of fiber thickness could be specific for each cell type and needs to be optimized for the tissue being developed.[28,40]

In this study, cell growth of MDA-MB-231, ADSC and EPC was studied on random-oriented nanofibers, microfibers and

aligned-nanofiber matrices. Cell proliferation of MDA-MB-231 on all the 3D matrices were significantly lower than on 2D tissue culture plates, which was similar to Rabionet et al.[22a] Cell proliferation of MDA-MB-231 and ADSC was found to be significantly higher on all nanofiber than on microfiber matrices. The higher cell proliferation on nanofibers could be attributed to higher cellular adhesion compared to the microfibers, which had lower cell adhesion due to higher inter-fiber porosity. In contrast, significantly high cell proliferation of EPC could be observed on microfibers than on nanofibers. Further, higher cellular infiltration of all three cell types could be observed on the microfiber matrices than on nanofiber matrices due to its higher inter-fiber spacing, similar to other studies on microfibers.[49] Cellular infiltration of MDA-MB-231 was previously demonstrated in microfibers[22c] and those of endothelial cells,[50] which suggest that microfibers may stimulate invasive properties of MDA-MB-231 similar to tumor metastasis. On aligned matrices, all cell types appeared in elongated morphology with actin orientation along the fiber direction. Similar elongated morphology of cells on aligned fiber matrices was reported,[23,51] while a mixture of spherical and elongated cells could be observed in random-oriented matrices probably due to higher intersections of fibers.

To further characterize the growth of breast cancer cells on the PCL matrices, FUCCI-transfected MDA-MB-231 were cultured on the matrices. Thus MDA-MB-231 cells in different stages of cell cycle could be observed, showing that the matrices support the proliferation of the cancer cells. A higher percentage of green:red cells were found on microfibers than on nanofibers matrices, indicating that microfibers support better proliferation of cells. Further, MDA-MB-231 cells grown on the matrices were extracted to form mammospheres on low-adhesion plates. Mammosphere formation assay (MFA) displays the growth of the CSC population within the MDA-MB-231 cells[22a,38a] In this study, the MFI was similar on both PCL matrices as well as tissue-culture plates. Similarly, Feng et al.[38a] also demonstrated that the proportion of CSCs in MDA-MB-231 cultured on PCL does not increase dramatically in comparison to cells grown in 2D. Domura et al.[51] demonstrated that drug responses against MDA-MB-231 was similar on different topographies, thus concluding that cells grown on electrospun PCL matrices could be successfully used as models to test anti-cancer drugs. Since, microfiber matrices support better cellular growth of EPC, infiltration of all cell types, has lower stiffness than those of nanofiber matrices, and support the CSC population similar to nanofibers, microfiber matrices could be considered a scaffold of choice for the in vitro and in vivo models.

The second part of the study was to determine the effect of surface treatment on the growth of breast cancer cells, and two breast cancer-associated cell types on the electrospun PCL matrices. Surface treatment includes methods such as plasma treatment, UV irradiation and corona discharge, which influences the surface properties of the electrospun matrices namely hydrophilicity, surface roughness and elemental composition. Such modifications can remain on the surface of the material for more than a year[52] resulting in an increase of cellular interactions.[53] Plasma treatment involves the use of plasma of air or a mixture of different gases such as nitrogen, oxygen, argon

ADVANCED
SCIENCE NEWS

www.advancedsciencenews.com

ADVANCED
MATERIALS
INTERFACES

www.advmatinterfaces.de

Figure 7. Proliferation of EPC on electrospun PCL matrices. A) Proliferation of EPC over 12 d measured by WST-8 assay on random-oriented and aligned PCL fibers with and without plasma treatment ($n = 3$, mean $\pm$ SD). Top view of cell growth (DAPI (blue) and actin (green)) on B) nanofibers and C) aligned fibers (scale bar = 100 μm). Cross-sectional analysis of the cellular migration of EPC (overlay of phase-contrast and DAPI (blue)/actin (green) staining) on D) nanofibers (scale bar = 50 μm) and E) microfibers (scale bar = 100 μm) (* $p < 0.05$).

and ammonia to modify the surface and mechanical properties of electrospun matrices. It results in a decrease in the ultimate tensile strength and ultimate strain, and an increase in Young's modulus of the matrices.[53] It has been shown to have a positive effect on the growth of different cell types such as fibroblasts,[29d,52] limbal epithelial cells,[54] chondrocytes,[29c,55] human umblical vein endothelial cells (HUVEC)[33] and osteoblasts[29a,b,31b,53,56] on electrospun PCL matrices. In this study, UV and air-plasma treatment of the electrospun PCL matrices were characterized and the effect air-plasma treatment on the growth of breast cancer-associated cells on PCL matrices was tested.

After 150 s of treatment, the fibers were intact and the matrices became extremely hydrophilic, as confirmed by water contact angle measurements (≈0°). As air-plasma treatment was found to damage the matrices lesser and lead to higher hydrophilicity in comparison to UV over 150 s duration, air-plasma treatment for 150 s was preferred as a method of surface treatment for this study. The treatment had no significant effect on rat-tail collagen-I adhesion. C1s spectrum of the XPS analysis showed the presence of C−O and O=C−O functional groups at 286.6 and 289.0 eV of the pristine PCL matrices respectively identified according to the literature.[57] Air-plasma treatment lead to a decrease in carbon ratio and an increase in oxygen and nitrogen ratios (Figure 3) due to the formation of C=O and C−N functional groups indicated at 287.8 and 285.8 eV[57c] binding energy respectively. The O/C ratio increased from 0.28 to 0.46. Similar effect of air-plasma treatment on the O/C ratio, from 0.15 to 0.4 was reported by Herrera et al. which further determined the increase of oxygen-containing species, namely, −OH, O−C=O, and −COOH.[58]

Since the plasma-treated matrices are extremely hydrophilic, seeding the cell suspension directly on the matrices lead to a distribution of the cells where the cell adhesion was influenced by the hydrophilicity of the matrices. Hence, about 200 µL of media was added onto the matrices prior to adding the cell suspension. This removed the effect of hydrophilicity on cellular adhesion and the observed proliferation (WST-8 assay) results were just a function of cellular proliferation.

Cell growth of MDA-MB-231 and ADSC was similar on pristine and air-plasma treated PCL matrices. However, EPC showed significantly better growth on plasma-treated matrices indicating the preference of EPC to grow on highly hydrophilic surfaces. In this study, air-plasma treatment was found to render the matrices extremely hydrophilic (with a WCA approximately 0°). Webb et al.[59] and Lee et al.[60] concluded that a WCA of 20–55° is optimal for maximal cell adhesion on a substrate irrespective of the cell type, and is significantly reduced on extremely hydrophilic or hydrophobic substrates. Hence it would be of future interest to characterize moderately hydrophilic PCL surfaces, generated through the use of O_2 or N_2-plasma, for the enhanced proliferation of the breast cancer-associated cells.

The use of microfiber PCL matrices along with the air-plasma treatment has been shown to support the growth of all the three cell types used in the study, with the growth of EPC being significantly influenced by the air-plasma treatment. Further, the microfiber matrices had lower stiffness and enabled cellular infiltration. It would be of interest to generate organoids containing multiple cell types that self-assemble into physiological structures in vitro, which could be patient-derived or co-culture of different cell types along with the presence of ECM thus recreating the tumor microenvironment in vitro.[61] PCL matrices have been shown to be used successfully in the cultivation of patient-derived breast cancer organoids,[62] and in the generation of breast tumor organoids by co-culture of fibroblasts and breast cancer cells.[63]

ADSC have been shown to significantly enhance the tumorigenicity of MDA-MB-231 cells in vivo,[19,20a,64] while the culture of EPC has been shown to significantly enhance vascularization in PCL scaffolds.[25a,b] Hence, a co-culture of MDA-MB-231 cells, ADSC and EPC on plasma-treated microfiber matrices will enable the formation of tumoroids with a more physiological tumorigenicity and vascularization in vitro for subsequent drug testing. Plasma-functionalized electrospun PCL matrices have also been successfully tested as a substrate for implantation of mesenchymal stem cells in a rodent model of myocardial infarction.[65]

4. Conclusion

In this study, the role of fiber-thickness and plasma treatment of electrospun PCL matrices toward the in vitro growth of breast cancer associated cells namely MDA-MB-231, ADSC, and EPC have been studied. Microfibers supported the cell growth of all the three cell types, had lower stiffness and allowed enhanced cellular infiltration better than nanofiber matrices. Air-plasma treated PCL matrices had significant increase in surface oxygen concentration and hydrophilicity. The proliferation of EPC was significantly higher on plasma-treated matrices than on pristine matrices. In summary, we could show that plasma-treated electrospun PCL matrices support the growth of different breast cancer-associated cell types. From this data, we can conclude that plasma-treated PCL matrices are indicated as suitable 3D matrices for the generation of in vitro and in vivo breast cancer models containing multiple cell types.

5. Experimental Section

Materials: PCL (M_n = 80000 g mol^{-1}; Sigma-Aldrich, Saint Louis, MO, USA) was used. Chloroform (Merck Millipore, Billerica, MA, USA), ethanol (Carl Roth GmbH & Co. KG, Karlsruhe, Germany), glacial acetic acid (>99%; VWR, Radnor, PA, USA), and formic acid (99%; VWR) were used as solvents. MDA-MB-231 cells were obtained from ATCC (Manassas, VA, USA). ADSC and EPC were isolated from patient-derived tissue samples as described previously.[66] Human tissue collection was approved by the Ethics Committee of the Friedrich-Alexander University of Erlangen-Nürnberg (FAU) (Germany) (Ethics #264_13B, #424_18B) in accordance with the World Medical Association Declaration of Helsinki. Informed consent was obtained from all patients. Cell culture crowns were obtained from Sigma Aldrich. For cell culture, Dulbecco's Modified Eagle Medium (DMEM) High Glucose (Life technologies, Carlsbad, CA, USA), Minimum Essential Medium α (MEM α) (Life technologies), Endothelial Cell Growth Basal Medium-2 (EBM-2) (Lonza Group, Basel, Switzerland), fetal calf serum (FCS) (FBS superior, Biochrom GmbH, Berlin, Germany) were used.

Preparation of Polymer Solutions and Electrospinning of PCL Fibers: Depending on the requirements of matrices with different diameters and orientation, different solvents and electrospinning parameters that were

standardized by Stafiej et al.[11] and Balguid et al.[40] were used. In total, four different types of matrices were produced: PCL-random (nanofibers, micro/nanofibers, microfibers) and PCL-aligned nanofibers. For the production of random-oriented nanofibers, 0.6 g of PCL (80 KDa) was dissolved in a mixture of 3.5 mL of formic acid and 1.5 mL of acetic acid with a grounded aluminum foil used as a collector. An applied voltage of 15 kV, needle-to-collector distance of 17 cm and flow rate of 0.2 mL h⁻¹ were maintained. Similarly, other matrices were synthesized using the parameters summarized in Table 1. For aligned nanofibers, a rotating drum with bars at a distance of 24 cm, a rotational speed of 1000 rpm and a drum diameter of 20 cm was used as a dynamic collector. PCL was always dissolved for 4 to 5 h prior to electrospinning.

Surface Treatment: For surface treatment and cell culture, the electrospun matrices were treated with 70% ethanol and water to detach them from the aluminum foil. They were inserted into 24-well plate cell crowns. For analyzing the effect of surface treatment, matrices were UV-treated (60, 180, 300 s) (Model 30, Jelight Company Inc, Irvine, CA, USA) or air plasma-treated (150, 300, 450 s) (ILMVAC Plasma Clean 4, Gardner Denver, Milwaukee, Wisconsin, USA). The plasma cleaner had a constant power of 350 W and plasma was generated at a pressure of 250 Pa.

Characterization of the Electrospun PCL Matrices and Surface Treatment—Scanning Electron Microscopy of PCL Matrices: The electrospun matrices were examined by SEM (AURIGA CrossBeam; Carl Zeiss Microscopy GmbH, Oberkochen, Germany). Prior to microscopy the samples were coated with a 7.5 nm gold layer using a sputter coater (Q150T Turbo-pumped Sputter Coater, Quorum Technologies Inc., Guelph, ON, Canada). Diameter measurements were performed by measuring the diameters of 25 fibers on three different samples from different batches of each type.

Tensile Testing of Electrospun Matrices: Tensile testing of the random-oriented nanofibers and microfibers were conducted by using universal testing machine Z050 (ZwickRoell, Ulm, Germany), $n = 5$. Strips of electrospun matrices were cut in 30 mm length, and a width of 10 mm. Thickness of the nanofiber matrices varied from 22–55 µm, while those of microfiber matrices were 270–400 µm. Tests were performed with a grip-to-grip distance of 10 mm, and a strain rate of 1 mm min⁻¹. Young's modulus was determined by using a regression slope from 2% strain within the elastic region.

Tensile properties of the aligned-nanofibers were evaluated by combining the aligned fibers into a bundle ($n = 5$), as performed by Munawar et al.[67] and performing a longitudinal tensile test using Vibrodyn 500 (Lenzing Instruments, Gampern, Austria). Young's modulus (E) was determined using the following equation

$$E = k\rho L \div M \tag{1}$$

where k is the slope of the force-strain curve, ρ is the density of PCL, L is the gauge length, and M is the mass of the bundle.

XPS Analysis of Surface Treatment: Surface functionalization of plasma-treated samples were determined by XPS. Photoemission spectra were acquired using PHI Quantera II spectrometer (ULVAC-PHI, Inc., Chigasaki, Japan) equipped with monochromatized Al Kα X-ray source (1486.6 eV energy) and combined ion/electron charge neutralization gun. Spectra were fitted by Gaussian/Lorentzian convolution functions. Spectral background was optimized using a Shirley function simultaneously with spectral fitting.

Water Contact Angle: WCA measurements ($n = 2$) (OCA 20, DataPhysics Instruments GmbH, Filderstadt, Germany) were performed on the PCL matrices before and after UV and plasma treatment. Briefly, 4 µL drops of distilled water were added onto the fiber matrices. Pictures of the drops were taken 3 s after deposition and analyzed with the tangent leaning method to obtain the WCA for each matrix.

Fluorescence Staining of Surface Coatings: For analyzing the effect of UV and plasma treatment on collagen/fibrinogen adhesion, coating was performed by using 20 µL of 1.5 mg mL⁻¹ fluorescent fibrinogen solution (Invitrogen, Carlsbad, CA, USA) along with 50 µL of 4 mg mL⁻¹ rat-tail collagen type-I solution (Sigma-Aldrich) and 1.5 µL acetic acid diluted in

2.5 mL H₂O (milliQ), for 15 min. Images for comparison of fluorescent intensities of coating ($n = 3$) were obtained on a fluorescent microscope (Olympus IX83, cellSens Software, Olympus Corporation, Tokyo, Japan) with a standardized exposure for all matrices. To further determine the effect of 150 s of plasma-treatment on collagen-I adhesion on the PCL matrices by immunofluorescence, the collagen-I coated matrices were blocked in phosphate-buffered saline (PBS, Gibco, Waltham, MA, USA) with 5% goat serum for 30 min. It was followed by treatment with rabbit anti-rat collagen I (Bio-Rad Laboratories Inc., Hercules, CA, USA) (2 µg mL⁻¹, diluted in antibody diluent (Zytomed GmbH, Berlin, Germany)) for 1 h. After washing in PBS, Alexa Fluor 488 (Life Technologies) (goat anti-rabbit, 4 µg mL⁻¹, diluted in antibody diluent) was added. The matrices were imaged in a fluorescent microscope after washing.

Cell Culture of Breast Cancer-Associated Cells on Electrospun PCL Matrices—Cell Culture: The electrospun matrices were transferred to 24-well plate cell crowns for cell culture. Both nontreated and plasma-treated samples were sterilized by treatment with 70% ethanol for 20 min, followed by washing in PBS. Matrices were then dip-coated with rat-tail collagen-I (Sigma-Aldrich) at a concentration of 1 mg mL⁻¹ and incubated at 37 °C for 3 h. Prior to cell culture, matrices were washed three times in PBS.

The breast cancer cell line MDA-MB-231, primary ADSC and primary EPC were cultured on rat-tail collagen-I coated matrices with/without plasma-treatment [MDA-MB-231:nanofibers ($n = 3$), micro/nanofibers ($n = 3$), microfibers ($n = 3$), aligned nanofibers ($n = 3$), FUCCI-transfected cells ($n = 1$); primary ADSC:nanofibers ($n = 3$), microfibers ($n = 3$), aligned nanofibers ($n = 3$); primary EPC: nanofibers ($n = 3$), microfibers ($n = 3$), aligned nanofibers ($n = 1$)]. For all the cell types, each experiment was conducted in triplicates with 2.0×10^4 cells per matrix. MDA-MB-231 cells were cultured in DMEM (high glucose) supplemented with 10% FCS, 1% nonessential aminoacids, 1% L-glutamine and 1% penicillin/streptomycin. ADSC were cultured in alpha-MEM supplemented with 10% FCS and 1% pencillin/streptomycin. EPC were cultured in EBM-2 supplemented with Vascular endothelial growth factor (VEGF), basic fibroblast growth factor (bFGF), Insulin-like growth factor (IGF), Epidermal growth factor (EGF), hydrocortisol, ascorbic acid, heparin, 1% gentamycin sulfate/amphotericin B with 10% FCS. All cells were incubated at 37 °C and 5% CO₂. After 24 h, the supernatant was replaced by 1 mL of fresh media. Media was changed every 2 d.

Proliferation of Cultured Cells: In order to determine the effects of fiber diameter and plasma-treatment on the proliferation of MDA-MB-231, ADSC, and EPC, cells were cultured on respective matrices with or without plasma-treatment, in at least technical triplicates per experiment. Proliferation of the cells was measured on day 3, 6, 9, 12 by Colorimetric Cell Viability Kit I (CCVK-I) (WST-8, Promokine, Heidelberg, Germany). Cell culture media in each sample was replaced with 450 µL of the respective cell culture medium containing 45 µL of CCVK-I and incubated for 2 h at 37 °C and 5% CO₂. In triplicates, 100 µL of supernatant was transferred to a 96-well plate and the absorbance was measured at 450 nm (background at 600 nm) using a microplate reader. After carefully washing the matrices in PBS, fresh medium was added for further cultivation. Samples with absorbance below a cut-off value of 0.1 were eliminated from the calculations as they were considered nonrepresentative samples of cell growth, due to technical errors.

Gelatin Embedding and Cross-Sectioning of the Matrices: To determine the cellular migration into the matrices, seeded matrices were fixed using 4%-phosphate buffered formaldehyde (Carl Roth GmbH) at day 12, stained with DAPI (4′,6-diamidino-2-phenylindole, 1:10 000 in PBS) and ActinGreen488 ReadyProbes (Invitrogen) (1:50) for 30 min and embedded into gelatin.[68] A 5% gelatin solution with 5% glucose were dissolved in PBS and pre-warmed to 45 °C. The matrices were taken in a mold and the gelatin-embedding solution was poured onto it and incubated for 2 h. The samples were transferred to −80 °C for polymerization. The samples were then cryosectioned at −20 °C.

Confocal Microscopy: Cells on matrices were fixed on day 12 using 4% phosphate buffer paraformaldehyde and stained with DAP and ActinGreen. Cells were imaged using a confocal laser scanning

ADVANCED
SCIENCE NEWS
www.advancedsciencenews.com

ADVANCED
MATERIALS
INTERFACES
www.advmatinterfaces.de

microscope (Leica). F-Actin Alexa 488 was detected with an Argon laser at 488 nm, and DAPI was detected with a UV laser at 350 nm.

Generation of FUCCI Transfected MDA-MB-231: FastFUCCI expressing cell lines were produced by transfecting Lenti-X 293T cells (Takara, #632180) with pBOB-EF1-FastFUCCI-Puro (Addgene, #86849) and packaging plasmids (Addgene, #8454, #12260). The transfection was carried out using Lipofectamine 2000 reagent. The virus-containing supernatant was collected 48 h after transfection and precleaned by brief centrifuging. The medium was then concentrated ($10\times$) using the LentiX-concentrator (Takara, #631232). The concentrated virus-containing medium (10^7 infectious units mL^{-1}) was then used to transduce MDA-MB-231, which were seeded at a density of 1×10^5 per 9.6 cm^2, 24 h prior to transduction. After infection, successfully transduced stable MDA-MB-231 were further selected using puromycin (Gibco) (1 µg mL^{-1}). The FUCCI-transfected MDA-MB-231 cells were then cultured on the PCL nanofibers and microfibers matrices, and the ratio of red:green:yellow cells were counted ($n = 2$).

Mammosphere Formation Assay: After Day 12, MDA-MB-231 from different PCL matrices ($n = 3$; nanofibers, microfibers and aligned nanofibers) and 2D-culture ($n = 3$) as control were washed with PBS and detached with accutase (Sigma-Aldrich) at 37 °C and 5% CO$_2$. Cells were resuspended with DMEM/F12 medium (Gibco) containing the following supplements: B27 (Gibco), EGF (20 ng mL^{-1}; Sigma-Aldrich) and FGF (10 ng mL^{-1}; Miltenyi Biotec B.V. & Co. KG, Bergisch Gladbach, Germany), 1% L-glutamine. A suspension containing 2×10^3 cells per well was seeded onto a 6-well, ultralow attachment microplate (Corning, NY, USA) and incubated for 7 d at 37 °C and 5% CO$_2$. After 7 d, spherical mammospheres bigger than 50 µm were counted. The MFI of each culture condition was calculated as follows

$$\text{Mammosphere forming index, MFI}\,(\%) = \left(\frac{\text{number of mammospheres}}{\text{number of cells plated}} \right) \times 100$$

(2)

Statistical Analysis: All the experiments were performed in triplicates unless otherwise stated and the results were expressed as mean±standard deviation. For statistical analysis, a Kruskal–Wallis test was conducted and Mann–Whitney U test was used as a post-hoc test using SPSS. The WST-8 plots were constructed using Graphpad Prism 8 and the XPS plots using Origin 2017. Two sets of data were considered statistically different when $p \leq 0.05$.

Supporting Information

Supporting Information is available from the Wiley Online Library or from the author.

Acknowledgements

Conflict of Interest

The authors declare no conflict of interest.

Authors Contribution

S.S., D.W.S., and A.K.W. designed the study. S.S. conducted the experiments and wrote the manuscript. A.K.W. and P.L.S. critically reviewed the manuscript. R.S., A.W., P.L.S., L.F., and I.T. were instrumental in generation of the cells required for the study and review of the manuscript. E.K. conducted the XPS experiments and analysis. R.S., P.L.S., and A.W. performed confocal analyzes, A.A. and R.E.H. helped with the study design and revision of the manuscript.

Data Availability Statement

The data that support the findings of this study are available from the corresponding author upon reasonable request.

[1] a) U. V. Fritschen, B. Grill, J. Wagner, H. Schuster, I. Sukhova, R. E. Giunta, C. Heitmann, C. Andree, R. E. Horch, U. Kneser, G. Germann, *Handchirurgie, Mikrochirurgie, plastische Chirurgie: Organ der Deutschsprachigen Arbeitsgemeinschaft fur Handchirurgie: Organ der Deutschsprachigen Arbeitsgemeinschaft fur Mikrochirurgie der Peripheren Nerven und Gefasse* **2020**, *52*, 58; b) P. I. Heidekrueger, N. Moellhoff, R. E. Horch, J. A. Lohmeyer, M. Marx, C. Heitmann, H. Fansa, M. Geenen, C. J. Gabka, S. Handstein, L. Prantl, U. von Fritschen, *J. Clin. Med.* **2021**, 10; c) A. D. Bach, I. H. Morgenstern, R. E. Horch, *Med. Sci. Monit.* **2020**, *26*, e921329; d) D. Steiner, R. E. Horch, I. Ludolph, A. Arkudas, *Microsurgery* **2020**, *40*, 74.
[2] W. Yang, X. Wu, F. Zhou, *Med. Sci. Monit.* **2021**, *27*, e928919.
[3] D. Lee, C. Cha, *Mater. Sci. Eng., C* **2020**, *112*, 110932.
[4] S. Bersini, J. S. Jeon, G. Dubini, C. Arrigoni, S. Chung, J. L. Charest, M. Moretti, R. D. Kamm, *Biomaterials* **2014**, *35*, 2454.
[5] a) J. A. Belgodere, C. T. King, J. B. Bursavich, M. E. Burow, E. C. Martin, J. P. Jung, *Front. Bioeng. Biotechnol.* **2018**, 6; b) R. Schmid, S. K. Schmidt, R. Detsch, H. Horder, T. Blunk, S. Schrüfer, D. W. Schubert, L. Fischer, I. Thievessen, S. Heltmann-Meyer, D. Steiner, D. Schneidereit, O. Friedrich, A. Grüneboom, H. Amouei, H. Wajant, R. E. Horch, A. K. Bosserhoff, A. Arkudas, A. Kengelbach-Weigand, *Adv. Funct. Mater.* **2021**, 32.
[6] a) K. Guiro, T. L. Arinzeh, *Breast Cancer: Basic Clin. Res.* **2016**, *9s2*, BCBCR.S29424; b) S. Sant, P. A. Johnston, *Drug Discovery Today Technol.* **2017**, *23*, 27.
[7] a) N. Kanaya, G. Somlo, J. Wu, P. Frankel, M. Kai, X. Liu, S. V. Wu, D. Nguyen, N. Chan, M.-Y. Hsieh, M. Kirschenbaum, L. Kruper, C. Vito, B. Badie, J. H. Yim, Y. Yuan, A. Hurria, C. Peiguo, J. Mortimer, S. Chen, *J. Steroid Biochem. Mol. Biol.* **2017**, *170*, 65; b) E. Marangoni, M.-F. Poupon, *Curr. Opin. Oncol.* **2014**, *26*, 556.
[8] B. V. Jardim-Perassi, A. S. Arbab, L. C. Ferreira, T. F. Borin, N. R. Varma, A. S. Iskander, A. Shankar, M. M. Ali, D. A. de Campos Zuccari, *PLoS One* **2014**, *9*, e85311.
[9] I. Holen, V. Speirs, B. Morrissey, K. Blyth, *Dis. Models Mech.* **2017**, *10*, 359.
[10] S. Bimonte, A. Barbieri, G. Palma, D. Rea, A. Luciano, M. D'Aiuto, C. Arra, F. Izzo, *BioMed Res. Int.* **2015**, *2015*, 878134.
[11] P. Stafiej, F. Küng, D. Thieme, M. Czugala, F. E. Kruse, D. W. Schubert, T. A. Fuchsluger, *Mater. Sci. Eng., C* **2017**, *71*, 764.

[12] M. Barbarisi, G. Marino, E. Armenia, Q. Vincenzo, F. Rosso, M. Porcelli, A. Barbarisi, *J. Biomed. Mater. Res., Part A* **2015**, *103*, 1755.

[13] K. Ghosal, A. Manakhov, L. Zajickova, S. Thomas, *AAPS PharmSciTech* **2017**, *18*, 72.

[14] N. Siddiqui, S. Asawa, B. Birru, R. Baadhe, S. Rao, *Mol. Biotechnol.* **2018**, *60*, 506.

[15] G. Rijal, W. Li, *Biomaterials* **2016**, *81*, 135.

[16] a) S. Palomeras, M. Rabionet, I. Ferrer, A. Sarrats, M. Garcia-Romeu, T. Puig, J. Ciurana, *Molecules* **2016**, *21*, 537; b) G. M. Balachander, S. A. Balaji, A. Rangarajan, K. Chatterjee, *ACS Appl. Mater. Interfaces* **2015**, *7*, 27810.

[17] D. L. Holliday, V. Speirs, *Breast Cancer Res.* **2011**, 13.

[18] K. J. Chavez, S. V. Garimella, S. Lipkowitz, *Breast Dis.* **2010**, *32*, 35.

[19] E. Koellensperger, L. C. Bonnert, I. Zoernig, F. Marme, S. Sandmann, G. Germann, F. Gramley, U. Leimer, *Stem Cell Res. Ther.* **2017**, *8*, 121.

[20] a) R. Schweizer, W. Tsuji, V. S. Gorantla, K. G. Marra, J. P. Rubin, J. A. Plock, *Stem Cells Int.* **2015**, *2015*, 120949; b) M. G. S. Alessandra Bielli, P. Gentile, S. Agostinelli, C. Tarquini, V. Cervelli, a. A. Orlandi, **2014**, 345.

[21] M. Marcola, C. E. Rodrigues, *Stem Cells Int.* **2015**, *2015*, 832649.

[22] a) M. Rabionet, M. Yeste, T. Puig, J. Ciurana, *Polymers* **2017**, *9*, 328; b) C. S. Szot, C. F. Buchanan, P. Gatenholm, M. N. Rylander, J. W. Freeman, *Mater. Sci. Eng., C* **2011**, *31*, 37; c) K. Guiro, S. A. Patel, S. J. Greco, P. Rameshwar, T. L. Arinzeh, *PLoS One* **2015**, *10*, e0118724.

[23] S. Saha, X. Duan, L. Wu, P. K. Lo, H. Chen, Q. Wang, *Langmuir* **2012**, *28*, 2028.

[24] a) S. M. Safaeijavan R, A. Divsalar, A. Eidi, A. Ardeshirylajimi, *Iran. J. Basic Med. Sci.* **2014**, *17*, 903; b) C. Brannmark, A. Paul, D. Ribeiro, B. Magnusson, G. Brolen, A. Enejder, A. Forslow, *PLoS One* **2014**, *9*, e113620.

[25] a) J. K. Hong, J. Y. Bang, G. Xu, J. H. Lee, Y. J. Kim, H. J. Lee, H. S. Kim, S. M. Kwon, *Int. J. Nanomed.* **2015**, *10*, 1189; b) S. Singh, B. M. Wu, J. C. Dunn, *Tissue Eng., Part A* **2011**, *17*, 1819.

[26] M. Chen, P. K. Patra, S. B. Warner, S. Bhowmick, *Tissue Eng.* **2007**, *13*, 579.

[27] A. S. Badami, M. R. Kreke, M. S. Thompson, J. S. Riffle, A. S. Goldstein, *Biomaterials* **2006**, *27*, 596.

[28] C. A. Bashur, L. A. Dahlgren, A. S. Goldstein, *Biomaterials* **2006**, *27*, 5681.

[29] a) D. Yan, J. Jones, X. Y. Yuan, X. H. Xu, J. Sheng, J. C. Lee, G. Q. Ma, Q. S. Yu, *J. Biomed. Mater. Res., Part A* **2013**, *101*, 963; b) D. Sankar, K. T. Shalumon, K. P. Chennazhi, D. Menon, R. Jayakumar, *Tissue Eng., Part A* **2014**, *20*, 1689; c) A. Martins, E. D. Pinho, S. Faria, I. Pashkuleva, A. P. Marques, R. L. Reis, N. M. Neves, *Small* **2009**, *5*, 1195; d) S. M. Atyabi, F. Sharifi, S. Irani, M. Zandi, H. Mivehchi, Z. Nagheh, *Cell Biochem. Biophys.* **2016**, *74*, 181.

[30] E. G. Bajsić, B. Mijović, N. V. Penava, T. H. Grgurić, M. Slouf, E. Zdraveva, *J. Appl. Polym. Sci.* **2016**, *133*, 43539.

[31] a) E. D. Yildirim, D. Pappas, S. Güçeri, W. Sun, *Plasma Processes Polym.* **2011**, *8*, 256; b) Y.-M. Ko, D.-Y. Choi, S.-C. Jung, B.-H. Kim, *J. Nanosci. Nanotechnol.* **2015**, *15*, 192.

[32] W. Kosorn, B. Thavornyutikarn, P. Uppanan, P. Kaewkong, W. Janvikul, *Int. Proc. Chem., Biol. Environ. Eng.* **2012**, *43*, 44.

[33] N. Recek, M. Resnik, H. Motaln, T. Lah-Turnšek, R. Augustine, N. Kalarikkal, S. Thomas, M. Mozetič, *Int. J. Polym. Sci.* **2016**, *2016*, 7354396.

[34] a) W. Asghar, R. El Assal, H. Shafiee, S. Pitteri, R. Paulmurugan, U. Demirci, *Mater. Today* **2015**, *18*, 539; b) B. Weigelt, C. M. Ghajar, M. J. Bissell, *Adv. Drug Delivery Rev.* **2014**, *69–70*, 42; c) G. M. Balachander, R. Kotcherlakota, B. Nayak, D. Kedaria, A. Rangarajan, K. Chatterjee, *ACS Biomater. Sci. Eng.* **2021**, *7*, 3470.

[35] M. T. Nelson, A. Short, S. L. Cole, A. C. Gross, J. Winter, T. D. Eubank, J. J. Lannutti, *BMC Cancer* **2014**, *14*, 825.

[36] Y. M. Kook, H. Kim, S. Kim, C. Y. Heo, M. H. Park, K. Lee, W. G. Koh, *Nanomaterials* 117, **2018**, *8*.

[37] a) S. Singh, B. M. Wu, J. C. Dunn, *J. Biomed. Mater. Res., Part A* **2012**, *100*, 720; b) D. I. Braghirolli, V. E. Helfer, P. C. Chagastelles, T. P. Dalberto, D. Gamba, P. Pranke, *Biomed. Mater.* **2017**, *12*, 025003; c) Q. Li, Z. Wang, S. Zhang, W. Zheng, Q. Zhao, J. Zhang, L. Wang, S. Wang, D. Kong, *Mater. Sci. Eng., C* **2013**, *33*, 1646; d) M. Ahmed, T. Ramos, P. Wieringa, C. V. Blitterswijk, J. Boer, L. Moroni, *Sci. Rep.* **2018**, *8*, 6386.

[38] a) S. Feng, X. Duan, P. K. Lo, S. Liu, X. Liu, H. Chen, Q. Wang, *Integr. Biol.* **2013**, *5*, 768; b) J. Sims-Mourtada, R. A. Niamat, S. Samuel, C. Eskridge, E. B. Kmiec, *Int. J. Nanomed.* **2014**, *9*, 995.

[39] G. M. Balachander, P. M. Talukdar, M. Debnath, A. Rangarajan, K. Chatterjee, *ACS Appl. Mater. Interfaces* **2018**, *10*, 33814.

[40] M. A. Balguid, A, M. H. van Marion, R. A. Bank, C. V. Bouten, F. P. Baaijens, *Tissue Eng., Part A* **2009**, *15*, 437.

[41] a) D. W. Schubert, V. Allen, U. Dippel, *Adv. Eng. Mater.* **2021**, *23*; b) D. W. Schubert, *Macromol. Theory Simul.* **2019**, *28*.

[42] A. G. Guex, G. Fortunato, D. Hegemann, H. T. Tevaearai, M. N. Giraud, *Methods Mol. Biol.* **2013**, *1058*, 119.

[43] J. E. W. Patricia, J. Keely'*, S. A. Santoro, **1995**.

[44] S. Alowami, S. Troup, S. Al-Haddad, I. Kirkpatrick, P. H. Watson, *Breast Cancer Res.* **2003**, *5*, R129.

[45] a) T. T. Dao, N. B. Vu, L. H. Pham, L. Van Gia, H. T. Le, L. T. Phi, K. H. Bui, P. T. Le, P. Van Pham, *Adv. Exp. Med. Biol.* **2018**, *1084*, 45; b) Y. Duan, Z. Wang, W. Yan, S. Wang, S. Zhang, J. Jia, *J. Biomater. Sci.* **2007**, *18*, 1153; c) S. Sharif, J. Ai, M. Azami, J. Verdi, M. A. Atlasi, S. Shirian, A. Samadikuchaksaraei, *J. Biomed. Mater. Res., Part B* **2018**, *106*, 1578; d) Y. Z. Zhang, J. Venugopal, Z. M. Huang, C. T. Lim, S. Ramakrishna, *Biomacromolecules* **2005**, *6*, 2583; e) D. S. Yu, C. F. Lee, H. I. Chen, S. Y. Chang, *Int. J. Urol.* **2007**, *14*, 939.

[46] T. Hodgkinson, X. F. Yuan, A. Bayat, *J. Tissue Eng.* **2014**, *5*, 204173141455166.

[47] A. C. Bean, R. S. Tuan, *Biomed. Mater.* **2015**, *10*, 015018.

[48] a) M. Vashaghian, B. Zandieh-Doulabi, J. P. Roovers, T. H. Smit, *Tissue Eng., Part A* **2016**, *22*, 1305; b) D. M. Binulal NS, N. Selvamurugan, K. T. Shalumon, S. Suja, U. Mony, R. Jayakumar, S. V. Nair, *Tissue Eng., Part A* **2010**, *16*, 393.

[49] a) J. Wu, Y. Hong, *Bioact. Mater.* **2016**, *1*, 56; b) Q. P. Pham, U. Sharma, A. G. Mikos, *Biomacromolecules* **2006**, *7*, 2796.

[50] Y. G. Ko, J. H. Park, J. B. Lee, H. H. Oh, W. H. Park, D. Cho, O. H. Kwon, *Tissue Eng. Regener. Med.* **2016**, *13*, 343.

[51] R. Domura, R. Sasaki, Y. Ishikawa, M. Okamoto, *J. Funct. Biomater.* **2017**, *8*, 18.

[52] J. F. Sajjad Shafei, Z. Chen, C. S. Wong, M. Naebe, *Polymers* **2017**, *9*, 614.

[53] a) J. J. Da Yan, X. Yuan, X. Xu, J. Sheng, J. C. M. Lee, G. Ma, Q. Yu, *J. Med. Biol. Eng.* **2013**, *33*, 171; b) T. Jacobs, R. Morent, N. De Geyter, P. Dubruel, C. Leys, *Plasma Chem. Plasma Process.* **2012**, *32*, 1039.

[54] S. Sharma, D. Gupta, S. Mohanty, M. Jassal, A. K. Agrawal, R. Tandon, *Invest. Ophthalmol. Vis. Sci.* **2014**, *55*, 899.

[55] W. Zhu, N. J. Castro, X. Cheng, M. Keidar, L. G. Zhang, *PLoS One* **2015**, *10*, e0134729.

[56] H. J. Jeon, H. Lee, G. H. Kim, *J. Mater. Chem. B* **2015**, *3*, 3279.

[57] a) P. Louette, F. Bodino, J.-J. Pireaux, *Surf. Sci. Spectra* **2005**, *12*, 27; b) N. Vandencasteele, F. Reniers, *J. Electron Spectrosc. Relat. Phenom.* **2010**, *178*, 394; c) T. Jacobs, N. De Geyter, R. Morent, T. Desmet, P. Dubruel, C. Leys, *Surf. Coat. Technol.* **2011**, *205*, S543; d) A. G. A. P. Dementjev, M. C. M. S. de, K. I. M. van de, A. V. Naumkin, A. A. Serov, *Diamond Relat. Mater.* **2000**, *9*, 1904.

[58] L. A. Can-Herrera, A. Ávila-Ortega, S. de la Rosa-García, A. I. Oliva, J. V. Cauich-Rodríguez, J. M. Cervantes-Uc, *Eur. Polym. J.* **2016**, *84*, 502.

[59] V. H. Ken Webb, P. A. Tresco, *J. Biomed. Mater. Res.* **1998**, *41*, 422.

[60] G. K. Jin Ho Lee, J. W. Lee, H. B. Lee, *J. Colloid Interface Sci.* **1998**, *205*, 323.

[61] a) J. Rodrigues, M. A. Heinrich, L. M. Teixeira, J. Prakash, *Trends Cancer* **2021**, *7*, 249; b) S. C. Mohan, T. Y. Lee, A. E. Giuliano, X. Cui, *Front. Bioeng. Biotechnol.* **2021**, *9*, 745943; c) H. Fan, U. Demirci, P. Chen, *J. Hematol. Oncol.* **2019**, *12*, 142; d) A. O. Sasmita, Y. P. Wong, *Int. J. Oncol. Res.* **2018**, *1*, 008; e) F. Keller, R. Rudolf, M. Hafner, *J. Cell. Biotechnol.* **2019**, *5*, 89; f) P. A. Mollica, E. N. Booth-Creech, J. A. Reid, M. Zamponi, S. M. Sullivan, X. L. Palmer, P. C. Sachs, R. D. Bruno, *Acta Biomater.* **2019**, *95*, 201; g) G. Rijal, W. Li, *Sci. Adv.* **2017**, *3*, e1700764.

[62] B. Nayak, G. M. Balachander, S. Manjunath, A. Rangarajan, K. Chatterjee, *Colloids Surf., B* **2019**, *180*, 334.

[63] a) A. Malakpour-Permlid, I. Buzzi, C. Hegardt, F. Johansson, S. Oredsson, *Sci. Rep.* **2021**, *11*, 6655; b) A. Malakpour-Permlid, S. Oredsson, *Toxicol. Rep.* **2021**, *8*, 627.

[64] B. G. Rowan, J. M. Gimble, M. Sheng, M. Anbalagan, R. K. Jones, T. P. Frazier, M. Asher, E. A. Lacayo, P. L. Friedlander, R. Kutner, E. S. Chiu, *PLoS One* **2014**, *9*, e89595;

[65] A. G. Guex, A. Frobert, J. Valentin, G. Fortunato, D. Hegemann, S. Cook, T. P. Carrel, H. T. Tevaearai, M. N. Giraud, *Acta Biomater.* **2014**, *10*, 2996.

[66] a) A. Weigand, A. M. Boos, K. Tasbihi, J. P. Beier, P. D. Dalton, M. Schrauder, R. E. Horch, M. W. Beckmann, P. L. Strissel, R. Strick, *Breast Cancer Res.* **2016**, *18*, 32; b) A. Weigand, K. Tasbihi, P. L. Strissel, R. Strick, R. E. Horch, A. M. Boos, *Handchirurgie, Mikrochirurgie, plastische Chirurgie: Organ der Deutschsprachigen Arbeitsgemeinschaft fur Handchirurgie: Organ der Deutschsprachigen Arbeitsgemeinschaft fur Mikrochirurgie der Peripheren Nerven und Gefasse* **2017**, *49*, 111.

[67] M. A. Munawar, D. W. Schubert, *Int. J. Mol. Sci.* **2021**, *22*, 10295.

[68] D. A. Brown, Y. F. Chou, R. E. Beygui, J. C. Dunn, B. M. Wu, *J. Biomed. Mater. Res., Part B* **2005**, *72*, 79.